Structural Eng./Earthquake Eng., JSCE, Vol. 18, No. 1, 27s—39s, 2001 April
(J. Struct. Mech. Earthquake Eng., JSCE, No. 675/ I —55)

THEORETICAL SOLUTIONS ON INTERFACIAL STRESS TRANSFER OF EXTERNALLY BONDED STEEL/COMPOSITE LAMINATES

Hong YUAN[1], Zhishen WU[2] and Hiroyuki YOSHIZAWA[3]

[1]Ph. D., Department of Urban and Civil Engineering, Ibaraki University (Nakanarusawa 4-12-1, Hitachi 316-8511, Japan)

[2]Member of JSCE, Dr. Eng., Associate Professor, Department of Urban and Civil Engineering, Ibaraki University (Nakanarusawa 4-12-1, Hitachi 316-8511, Japan)

[3]M. Eng., Nippon Steel Composite Co., Ltd. (Nihonbashikobuna-cho 3-8, Chuo-ku, Tokyo, Japan)

To effectively and efficiently utilize steel/FRP plates or sheets in strengthening civil infrastructures, a design strategy integrating the FRP properties and composite structural behavior needs to be adopted. The interfacial stress transfer behavior including debonding should be considered to be one of the most important effects on the composite structural behavior. In this paper, varieties of nonlinear interfacial constitutive laws, describing the pre- and post-cracking behaviour of FRP-concrete interface are introduced to solve the nonlinear interfacial stress transfer problems. Expressions for bonding capacity, interfacial shear stress distribution, initiation and propagation of interfacial crack are derived analytically.

Key Words: load-carrying capacity, FRP plates or sheets, interfacial fracture energy, effective bond length, debonding and softening

1. INTRODUCTION

To effectively and efficiently utilize the steel/composite plates or sheets, a design strategy integrating the properties of strengthening materials (steel/FRP plates or sheets) and composite structural behavior needs to be adopted. In strengthening deteriorated concrete structures, different failure modes have been reported[1]. There are several local failures due to interfacial fracture along FRP-concrete interface which frequently increase design constraints. Therefore, it is important to understand deeply the nature of bonding and debonding mechanism.

The interfacial stress distributions vary theoretically with thickness, elastic modulus and interfacial concrete behavior etc. Because of the complexity of composite and nonlinear interfacial behavior, the interfacial stress distributions are complex and also difficult to determine accurately by experimental investigation. Täljsten[2] presents the use of a linear and nonlinear fracture mechanics (NLFM) approach for the plate bonding technique. A derivation of the shear and peeling stresses in the adhesive layer of a beam with a strengthening plate bonded to its soffit and loaded with an arbitrary point load are presented in another literature by the same author[3]. Roberts[4] describes a two-stage analytical procedure for determining the distribution of shear and normal stresses in a variety of adhesive joints subjected to bending and axial forces. As for reinforced concrete beams, Roberts[5] gives a simple, approximate procedure for predicting the shear and normal stress concentrations in the adhesive layer of laminate beams. Brosens and Gemert[6] derive expressions for the anchoring capacity in both the serviceability and the ultimate limit state. The nonlinear concrete properties describing the pre- and post-cracking behavior are considered. Triantafillou[7] presents fracture mechanics procedures for mechanisms associated with premature bond failures of FRP-concrete interface. The implementation of these procedures in practical design equations is also demonstrated.

Saadatmanesh and Malek[8] develop a closed form solution for calculating shear and peeling stresses at the interface of the FRP plate and adhesive layer. Shear stress concentration in the adhesive layer around the flexural cracks has been included in the study. Malek et al.[9] present a method for calculating shear and normal stress concentrations at the cutoff point of the plate. The effect of the large flexural cracks along the beam has also been investigated. Wu and Yoshizawa[10] adopt the fracture energy approach to predict the composite behavior of reinforced concrete specimens strengthened with FRP sheet, and to explain the fact that less or no frictional and interlocking effects along the FRP-concrete interface could be observed. The predicted results such as load-deformation relationships and crack width are in close agreement with the experimental results. It is worth mentioning that Wu and Yoshizawa are the first to point out the softening behavior of concrete in shear based on the experimental observations. Yin and Wu [11] carry out a numerical simulation for simple shear and flexural tests with the FEM to verify the interface crack model with strain softening and the composite behavior of FRP-strengthened structures including debonding and concrete cracking propagation. It is found that the interfacial fracture energy is the most important parameter for the bond behavior and the ultimate load can be expressed in terms of the fracture energy. Recently, many studies have been carried out to investigate the FRP bonding and debonding mechanism through the simple shear test[12), 13), 14)]. Kamiharako et al.[12), 13)] propose the constitutive model for simulating bonding and debonding behavior of FRP sheet based on the experiment of continuous fiber sheet (CF sheet) bonded on concrete. Sato et al. [14)] develop a bond-slip-strain relation for carbon fiber sheet based on the bond characteristic and demonstrate its applicability to simulate the actual bond behavior. Through their research works it is found that the shear stress-slip relationship with a softening behavior can represent well the initiation and propagation of interfacial cracks.

Although a lot of researches have been made as reviewed above, the theoretical problems of interfacial stress transfer in steel plate- and FRP-strengthened structures are not well solved until now. The reason should be imputed to the complexity in mathematics when softening behavior is considered. A simpler case (adhesive bonded joint) is analyzed here to gain insight into the mechanics of FRP-concrete interface. Stresses in adhesive bonded joint are determined by the strength of material approach, where NLFM approach is introduced. Closed-form solutions are obtained for four cases of assumed interfacial stress-slip law. The post-peak softening is shown to lead to localization of slip and interfacial shear fracturing propagation with a process zone of finite length. This zone propagates along the interface during the loading process, causing the distribution of interfacial shear stress to become strongly nonuniform. The solution to this simpler problem brings some good understanding of the mechanics of FRP-strengthened structures that is useful for the FRP reinforcing design.

2. FUNDAMENTAL INTEFACE MODELS

FRP-strengthened concrete structures when loaded in bending and shearing can fail in several ways and show very complicated failure phenomena. These failure types can be grouped into six distinct categories: (a) steel yield and FRP rupture; (b) concrete compression failure; (c) shear failure; (d) debonding of layer along rebar; (e) delamination of FRP sheet; (f) peeling due to shear crack. Among these, the most complicated failure mode for FRP-strengthened structures is the delamination due to the unstable propagation of interfacial debonding initiating from the flexural or shear crack of concrete and/or various kinds of interlaminar defects. Therefore, the fracture mechanics based on energy consideration is considered to be very powerful for evaluating the load-carrying capacity and other composite behavior of the FRP-strengthened structures.

The adhesive bonded joint analyzed, shown in **Fig. 1**, may be thought as a simple and typical model of FRP-strengthened structures to understand the stress transfer and debonding behavior. The adhesive layer is mainly subjected to shear (mode II fracture). Thickness and width of the two layers are t_1 and b_1 for the upper steel/FRP laminate, and t_2 and b_2 for the lower concrete plate, respectively. The Young's moduli of the steel/FRP laminate and the concrete plate are E_1 and E_2, repectively. L is the bonding length. Before starting the derivations we make the following assumptions for simplicity

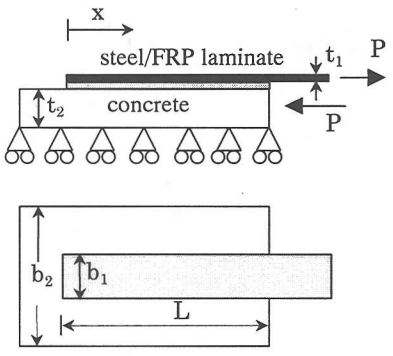

Fig. 1 Adhesive bonded joint

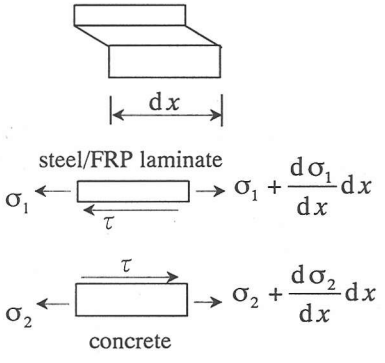

Fig. 2 Deformation and stresses of bonded joint

of the problems:

- ♦The adherents are homogeneous and linear elastic;
- ♦The adhesive is assumed as a medium of negligible thickness and only transfers the shear stress from FRP to concrete;
- ♦Bending effects are neglected;
- ♦The normal stresses are uniformly distributed over the cross-section;
- ♦The thickness and width of the adherents are constant throughout the bond line.

Considering the element shown in **Fig. 2**, the equations of equilibrium for adherents can be written as

$$\frac{d\sigma_1}{dx} - \frac{\tau}{t_1} = 0 \tag{1}$$

$$\sigma_1 t_1 b_1 + \sigma_2 t_2 b_2 = 0 \tag{2}$$

where τ is the shear stress in the adhesive layer. The constitutive equations for the adhesive layer and the two adherents are expressed as

$$\tau = f(\delta) \tag{3}$$

where δ is defined as the relative displacement between adherents $\delta = u_1 - u_2$.

$$\sigma_1 = E_1 \frac{du_1}{dx} \tag{4}$$

$$\sigma_2 = E_2 \frac{du_2}{dx} \tag{5}$$

Substituting equations (2)-(5) into equation (1) yields, by introducing two parameters of local bond strength τ_f and interfacial fracture energy G_f

$$\frac{d^2\delta}{dx^2} - \frac{2G_f}{\tau_f^{\,2}}\lambda^2 f(\delta) = 0 \tag{6}$$

$$\sigma_1 = \frac{\tau_f^{\,2}}{2G_f t_1 \lambda^2}\frac{d\delta}{dx} \tag{7}$$

where

$$\lambda^2 = \frac{\tau_f^{\,2}}{2G_f}\left(\frac{1}{E_1 t_1} + \frac{b_1}{b_2 E_2 t_2}\right) \tag{8}$$

It should be noted that equations similar to equation (6) have been successfully used to model the bond-slip mechanism between embedded reinforcing bars and concrete[15), 16), 17), 18)].

The four models of stress-slip relationship ($\tau - \delta$), as shown in **Fig. 3**, which are considered to be possible in representing the nonlinear interfacial behavior, are introduced here. It is noted that the area below the $\tau - \delta$ curve represents interfacial fracture energy of mode II, G_f, which is defined as the energy required to bring a local bond element to shear fracture (debonding).

Model I

$$f(\delta) = \begin{cases} \dfrac{\tau_f^{\,2}}{2G_f}\delta & when\ \ 0 \le \delta \le \delta_f \\ 0 & when\ \ \delta > \delta_f \end{cases}$$

As shown in **Fig. 3**a, the stress-slip relation is linearly ascending before the occurrence of

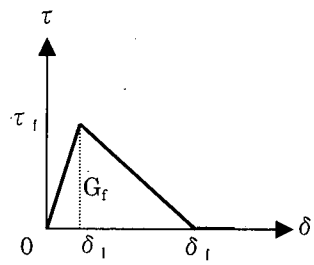

(b) model Ⅱ

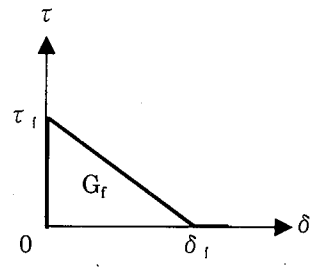

(c) model Ⅲ

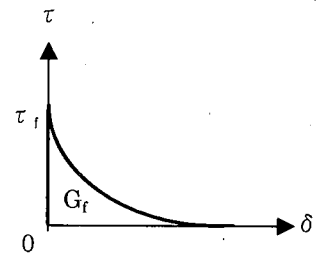

(d) model Ⅳ

Fig. 3 Different simplified shapes of τ - δ curves

interfacial fracture and the value of shear stress suddenly drops to zero when the value of slip exceeds δ_f without consideration of softening behavior.

Model Ⅱ

$$f(\delta)=\begin{cases}\dfrac{\tau_f}{\delta_1}\delta & when\ \ 0\le\delta\le\delta_1\\ \dfrac{\tau_f}{\delta_f-\delta_1}(\delta_f-\delta) & when\ \ \delta_1<\delta\le\delta_f\\ 0 & when\ \ \delta>\delta_f\end{cases}$$

As shown in **Fig. 3**b, the stress-slip relation is linearly ascending when the value of slip is smaller than δ_1. After the occurrence of interfacial fracture the stress-slip relation is linearly descending in a range of δ_1 to δ_f. And the value of shear stress reduces to zero when the value of slip exceeds δ_f.

Model Ⅲ

$$f(\delta)=\begin{cases}f(\delta)=\tau_f\left(1-\dfrac{\tau_f}{2G_f}\delta\right) & when\ \ 0\le\delta\le\delta_f\\ 0 & when\ \ \delta>\delta_f\end{cases}$$

Fig. 3c, which is a good approximation to model Ⅱ by omitting the ascending linear part because δ_1 is often much less than δ_f, shows a linearly descending stress-slip relation when the value of slip is smaller than δ_f. And the value of shear stress reduces to zero when the value of slip exceeds δ_f.

Model Ⅳ

$$f(\delta)=\tau_f\exp\left(-\frac{\tau_f}{G_f}\delta\right)$$

As shown in **Fig. 3**d, the stress-slip relation has an exponential softening behavior and the value of shear stress gradually descends to zero with the increase of slip.

3. THEORETICAL DERIVATIONS

In what follows the four models of stress-slip law are introduced to derive the shear stresses along the length in the bond zone in detail.

(1) Model Ⅰ: linear interfacial shear stress-slip relationship with a sudden stress drop

Substituting the relationship as shown in **Fig. 3**a for the case of $\delta\le\delta_f$ into equation (6), we obtain

$$\frac{d^2\delta}{dx^2}-\lambda^2\delta=0 \qquad (9)$$

The similar bond-slip relationship between reinforcing bars and concrete has been used by Yoshikawa and Tanabe[15], Wu[17] and Wu et al.[18].

The boundary conditions can be given as follows

$$\sigma_1 = 0 \text{ at } x = 0,$$

$$\sigma_1 = \frac{P}{b_1 t_1} \text{ at } x = L \qquad (10)$$

The solution of equation (9) for relative shear displacement, shear stress of adhesive layer and normal stress of laminate can be written in the form

$$\delta = A\cosh(\lambda x) + B\sinh(\lambda x) \qquad (11)$$

$$\tau = \frac{\tau_f^{\,2}}{2G_f}\left[A\cosh(\lambda x) + B\sinh(\lambda x)\right] \qquad (12)$$

$$\sigma_1 = \frac{\tau_f^{\,2}}{2G_f \lambda t_1}\left[A\sinh(\lambda x) + B\cosh(\lambda x)\right] \qquad (13)$$

The unknown constants in above equations can be solved by substituting the boundary conditions

$$A = \frac{2G_f}{\tau_f^{\,2}} \frac{P\lambda}{b_1 \sinh(\lambda L)}, \quad B = 0 \qquad (14)$$

Rewriting equations (11), (12) and (13) yields

$$\delta = \frac{2G_f}{\tau_f^{\,2}} \frac{P\lambda\cosh(\lambda x)}{b_1 \sinh(\lambda L)} \qquad (15)$$

$$\tau = \frac{P\lambda}{b_1} \cdot \frac{\cosh(\lambda x)}{\sinh(\lambda L)} \qquad (16)$$

$$\sigma_1 = \frac{P\sinh(\lambda x)}{b_1 t_1 \sinh(\lambda L)} \qquad (17)$$

when $\tau = \tau_f$ at $x = L$, P reaches its maximum value

$$P_{\max} = \frac{\tau_f b_1}{\lambda}\tanh(\lambda L) \qquad (18)$$

Substituting equation (18) into equation (16), we obtain interfacial shear stress distribution at maximum load value of P

$$\tau = \tau_f \frac{\cosh(\lambda x)}{\cosh(\lambda L)}$$

For large values of L, equation (18) converges to

$$P_{\max} = \frac{\tau_f b_1}{\lambda}$$

Crack propagation occurs when $\delta > \delta_f$. It can be studied by decreasing the values of bonding length L.

(2) Model Ⅱ: $\tau - \delta$ relationship with linearly ascending and descending branches

Substituting the relationship as shown in **Fig. 3**b into equation (6), we obtain

$$\frac{d^2\delta}{dx^2} - \lambda_1^{\,2}\delta = 0 \quad for \quad 0 \le \delta \le \delta_1 \qquad (19)$$

$$\frac{d^2\delta}{dx^2} + \lambda_2^{\,2}\delta = \lambda_2^{\,2}\delta_f \quad for \quad \delta_1 < \delta \le \delta_f \qquad (20)$$

where

$$\lambda_1^{\,2} = \lambda^2 \frac{2G_f}{\delta_1 \tau_f} = \frac{\tau_f}{\delta_1}\left(\frac{1}{E_1 t_1} + \frac{b_1}{b_2 E_2 t_2}\right)$$

$$\lambda_2^{\,2} = \lambda^2 \frac{2G_f}{(\delta_f - \delta_1)\tau_f} = \frac{\tau_f}{\delta_f - \delta_1}\left(\frac{1}{E_1 t_1} + \frac{b_1}{b_2 E_2 t_2}\right)$$

For $0 \le \delta \le \delta_1$, the solution of equation (19) can be derived as follows with similar form of equations (11), (12) and (13)

$$\delta = A\cosh(\lambda_1 x) + B\sinh(\lambda_1 x) \qquad (21)$$

$$\tau = \frac{\tau_f}{\delta_1}\left[A\cosh(\lambda_1 x) + B\sinh(\lambda_1 x)\right] \qquad (22)$$

$$\sigma_1 = \frac{\tau_f^{\,2}\lambda_1}{2G_f t_1 \lambda^2}\left[A\sinh(\lambda_1 x) + B\cosh(\lambda_1 x)\right] \qquad (23)$$

Moreover, for $\delta_1 < \delta \le \delta_f$, the solution of equation (20) can be derived in the form

$$\delta = C\sin[\lambda_2(x-L+a)] + D\cos[\lambda_2(x-L+a)] + \delta_f \quad (24)$$

$$\tau = -\frac{\tau_f}{\delta_f - \delta_1}\{C\sin[\lambda_2(x-L+a)] + D\cos[\lambda_2(x-L+a)]\} \quad (25)$$

$$\sigma_1 = \frac{\tau_f{}^2\lambda_2}{2G_f t_1\lambda^2}\{C\cos[\lambda_2(x-L+a)] - D\sin[\lambda_2(x-L+a)]\} \quad (26)$$

where a is the softening zone (micro-crack) length. The constants A, B, C and D in above equations are determined by the substitution of boundary and continuous conditions. The conditions can be written as

$$\sigma_1 = 0 \quad at \quad x = 0 \quad (27)$$

$$\sigma_1 \ is\ continuous\ at\ x = L - a \quad (28)$$

$$\delta = \delta_1 \ or\ \tau = \tau_f \ at\ x = L - a \quad (29)$$

$$\sigma_1 = \frac{P}{t_1 b_1} \ at\ x = L \quad (30)$$

Therefore, we have

$$A = \frac{\delta_1}{\cosh[\lambda_1(L-a)]}$$

$$B = 0$$

$$C = \frac{\lambda_1}{\lambda_2}\delta_1 \tanh[\lambda_1(L-a)]$$

$$D = \delta_1 - \delta_f$$

Finally, we obtain for $0 \le \delta \le \delta_1$

$$\delta = \delta_1 \frac{\cosh(\lambda_1 x)}{\cosh[\lambda_1(L-a)]} \quad (31)$$

$$\tau = \tau_f \frac{\cosh(\lambda_1 x)}{\cosh[\lambda_1(L-a)]} \quad (32)$$

$$\sigma_1 = \frac{\tau_f}{t_1\lambda_1}\cdot\frac{\sinh(\lambda_1 x)}{\cosh[\lambda_1(L-a)]} \quad (33)$$

and for $\delta_1 < \delta \le \delta_f$

$$\delta = (\delta_f - \delta_1)\left\{\frac{\lambda_2}{\lambda_1}\tanh[\lambda_1(L-a)]\times \sin[\lambda_2(x-L+a)] - \cos[\lambda_2(x-L+a)] + \frac{\delta_f}{\delta_f - \delta_1}\right\} \quad (34)$$

$$\tau = -\tau_f\left\{\frac{\lambda_2}{\lambda_1}\tanh[\lambda_1(L-a)]\sin[\lambda_2(x-L+a)] - \cos[\lambda_2(x-L+a)]\right\} \quad (35)$$

$$\sigma_1 = \frac{\tau_f}{\lambda_2 t_1}\left\{\frac{\lambda_2}{\lambda_1}\tanh[\lambda_1(L-a)]\cos[\lambda_2(x-L+a)] + \sin[\lambda_2(x-L+a)]\right\} \quad (36)$$

Substituting equation (30) into equation (36), we obtain

$$P = \frac{\tau_f b_1}{\lambda_2}\left\{\frac{\lambda_2}{\lambda_1}\tanh[\lambda_1(L-a)]\cos(\lambda_2 a) + \sin(\lambda_2 a)\right\} \quad (37)$$

It is obvious that P reaches maximum value when $\frac{dP}{da} = 0$ for general case or for simplicity, when $\tau = 0$ at $x = L$ for large value of bonding length. Therefore, a at maximum load can be found from the relation

$$\frac{1}{\tanh[\lambda_1(L-a)]} = \frac{\lambda_2}{\lambda_1}\tan(\lambda_2 a) \quad (38)$$

Substituting equation (38) into equation (37), we obtain

$$P_{\max} = \frac{\tau_f b_1}{\lambda_2}\left\{\frac{\delta_1}{\delta_f - \delta_1}\tanh^2[\lambda_1(L-a)]+1\right\} \cdot \sin(\lambda_2 a) \quad (39)$$

The problem in this model is that a is defined as an implicit function and can only be found by iteration. However it can be shown that for large values of L, equation (39) converges to

$$P_{\max} = \frac{\tau_f b_1}{\lambda}$$

which is the same with model Ⅰ.

Crack propagation occurs when $\delta > \delta_f$. It can be studied by decreasing the values of bonding length L. For large values of L, by letting $\delta = \delta_f$ at load end $x = L$ in equation (34), we obtain the maximum value of a that is associated with the initiation of macro-crack (debonding)

$$a_{\max} = \frac{1}{\lambda_2}\arctan\left(\frac{\lambda_1}{\lambda_2}\right)$$

(3) Model Ⅲ: $\tau - \delta$ relationship with only linearly descending branch

As for this model, there is no relative shear displacement until the maximum shear stress τ_f occurs at load end $x = L$. And the relative shear displacement increases gradually with the maximum shear stress shifts from load end to the other end of laminates. Substituting the relationship as shown in **Fig. 3**c for the case of $\delta \le \delta_f$ into equation (6), we obtain

$$\frac{d^2\delta}{dx^2} + \lambda^2\delta = \lambda^2\frac{2G_f}{\tau_f} \quad (40)$$

The solution of equation (40) for relative shear displacement, shear stress of adhesive layer and normal stress of laminate can be written in the form

$$\delta = A\sin\lambda[x-(L-a)] + B\cos\lambda[x-(L-a)] + \frac{2G_f}{\tau_f} \quad (41)$$

$$\tau = -\frac{\tau_f^2}{2G_f}\{A\sin\lambda[x-(L-a)] + B\cos\lambda[x-(L-a)]\} \quad (42)$$

$$\sigma_1 = \frac{\tau_f^2}{2G_f\lambda t_1}\{A\cos\lambda[x-(L-a)] - B\sin\lambda[x-(L-a)]\} \quad (43)$$

At the cross section with no interface slip (no shear micro-crack), the interfacial shear displacement and normal stresses in the steel/FRP and the concrete are equal to zero. At micro-crack tip we always have $\tau = \tau_f$, $\delta = 0$. And we can also infer from equilibrium of steel/FRP element that $\sigma_1 = 0$ at micro-crack tip. Assuming that micro-crack (softening zone) length is a, we can write the boundary conditions as follows

$$\sigma_1 = 0,\ \delta = 0 \text{ at } x = L - a \quad (44)$$

Therefore, the unknown constants A and B are obtained as

$$A = 0,\ B = -\frac{2G_f}{\tau_f}$$

Substituting these constants into equations (41)-(43) leads to

$$\delta = \frac{2G_f}{\tau_f}\{1-\cos\lambda[x-(L-a)]\} \quad (45)$$

$$\tau = \tau_f\cos\lambda[x-(L-a)] \quad (46)$$

$$\sigma_1 = \frac{\tau_f}{\lambda t_1}\sin\lambda[x-(L-a)] \quad (47)$$

Therefore, interfacial shear displacement, shear stress and normal stress in steel/FRP laminate are related with a. The value of a can be determined by the load value of P at load end. According to

$$\sigma_1 = \frac{P}{t_1 b_1} \text{ at } x = L$$

We obtain

$$P = \frac{\tau_f b_1}{\lambda}\sin(\lambda a) \qquad (48)$$

If $L \geq a_{max} = \frac{\pi}{2\lambda}$, then P reaches maximum at $a = a_{max}$, that is

$$P_{max} = \frac{\tau_f b_1}{\lambda} \qquad (49)$$

And then $\tau = 0$ at $x = L$.

If $L < a_{max}$ then P reaches maximum at $a = L$, that is

$$P_{max} = \frac{\tau_f b_1}{\lambda}\sin(\lambda L) \qquad (50)$$

Then $\tau = \tau_f \cos\lambda L \neq 0$ at $x = L$.

Crack propagation occurs when $\delta > \delta_f$. It can be studied by decreasing the values of bonding length L. a_{max} is associated with the initiation of macro-crack (debonding).

(4) Model Ⅳ: $\tau - \delta$ relationship with only exponential softening branch

Substituting the relationship as shown in **Fig. 3**d for the case of $\delta \leq \delta_f$ into equation (6), we obtain

$$\frac{d^2\delta}{dx^2} - \lambda^2 \frac{2G_f}{\tau_f}\exp\left(-\frac{\tau_f}{G_f}\delta\right) = 0 \qquad (51)$$

Similar with model Ⅲ, we have boundary conditions

$$\sigma_1 = 0 \text{ and } \delta = 0 \text{ at } x = L - a$$

and solving equation (51), we obtain

$$\delta = \frac{2G_f}{\tau_f}\ln\{\cosh[\lambda(x - L + a)]\} \qquad (52)$$

$$\tau = \frac{\tau_f}{\{\cosh[\lambda(x - L + a)]\}^2} \qquad (53)$$

$$\sigma_1 = \frac{\tau_f}{\lambda t_1}\tanh[\lambda(x - L + a)] \qquad (54)$$

Again, interfacial shear displacement, shear stress and normal stress in steel/FRP laminate are related with a. The value of a can be determined by the load value of P at load end. According to

$$\sigma_1 = \frac{P}{t_1 b_1} \text{ at } x = L$$

We obtain

$$P = \frac{\tau_f b_1}{\lambda}\tanh(\lambda a) \qquad (55)$$

Therefore, P reaches maximum value at $a = L$, that is

$$P_{max} = \frac{\tau_f b_1}{\lambda}\tanh(\lambda L) \qquad (56)$$

which is the same as equation (18). So for large values of L, equation (56) converges to

$$P_{max} = \frac{\tau_f b_1}{\lambda}$$

Let $a = L$ in equation (53), we obtain interfacial shear stress distribution at maximum value of P

$$\tau = \frac{\tau_f}{[\cosh(\lambda x)]^2}$$

Crack propagation occurs when P attains 97% of P_{max}. Taking into account that $\tanh(2) \approx 0.97$, following equation can be derived

$$a_{max} = \frac{2}{\lambda}$$

4. NUMERICAL RESULTS

(1) Shear stress distribution and crack propagation along interface

Based on above theoretical derivations, we first discuss numerically on shear stress distribution and crack propagation along interface of a single-lap pure shear test as shown in **Fig. 1**. Different following stages of shear stress distributions are represented in **Fig. 4**, which are associated with different models of stress-slip law.

As shown in **Fig. 4**, section Ⅰ is called the elastic stress state, and there is no interfacial crack or micro-crack (softening zone) along FRP-concrete interface. Section Ⅱ is called the softening state, and the interface is micro-cracked but still able to transfer shear stress. In section Ⅲ an interfacial crack (debonding) without stress transfer occurs. The detail discussion may be made as follows.

- Model Ⅰ At small loads, there is no interfacial debonding or softening along FRP-concrete interface as long as the interfacial shear stress at the end $x = L$ is less than τ_f. The maximum transferable force appears when the shear stress reaches the value τ_f at the end. After this the debonding at the end appears and the crack propagation happens, the shear stress peak (bond strength) τ_f moves towards the other end of the bonded joint, and the whole interface is in an elastic-debonding stage.
- Model Ⅱ At small loads, there is no interfacial debonding or softening along FRP-concrete interface as long as the interfacial shear stress at the end $x = L$ is less than τ_f. After shear stress attains τ_f $(\delta = \delta_1)$ at the end, the softening appears at the end, the whole FRP-concrete interface is in a combined elastic-softening stage, the load P increases with the increase of softening zone length a, and the maximum transfreable load appears at this stage. Debonding initiates when the softening zone length attains $a_{\max}$ $(\delta = \delta_f$ and $\tau = 0$ at $x = L)$. After this the crack propagation happens, the whole FRP-concrete interface is in a combined elastic-softening-debonded stage, and the shear stress peak τ_f moves towards the other end of the bonded joint. At certain moment, the shear stress peak τ_f reaches the end $x = 0$ and the whole interface is in the softening-debonded stage. After this, the transferable load decreases until the joint completely fails.
- Model Ⅲ At small loads, the softening zone exists and the whole FRP-concrete interface is in a combined elastic-softening stage. The maximum transferable load appears and debonding initiates when the softening zone length attains $a_{\max}$ $(\delta = \delta_f$ and $\tau = 0$ at $x = L)$. After this the crack propagation happens, the whole FRP-concrete interface is in a combined elastic-softening-debonded stage, and the shear stress peak τ_f moves towards the other end of the bonded joint. At certain moment, the shear stress peak τ_f reaches the end $x = 0$, and the whole interface is in the softening-debonded stage. After this, the transferable load decreases until the joint completely fails.
- Model Ⅳ This case is simmilar with model Ⅲ, but the shear stress distribution is different. At small loads, the softening zone exists and the whole FRP-concrete interface is in a combined elastic-softening stage. The maximum transferable load appears and debonding initiates when the softening zone length attains $a_{\max}$ $(\tau = 0$ at $x = L)$. After this the crack propagation happens.

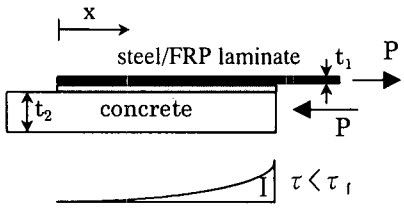

Before interfacial crack

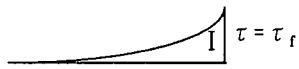

Crack initiation at x=L ($P=P_{max}$)

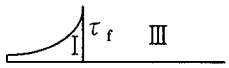

Crack propagation

(a) Model I

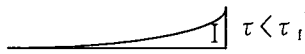

Before interfacial micro-crack

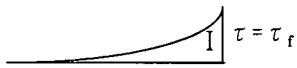

Micro-crack initiation at x=L

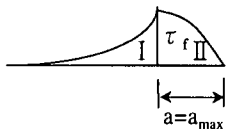

Crack initiation at x=L

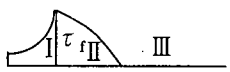

Crack propagation

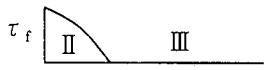

Crack propagation to the end of laminate

(b) Model II

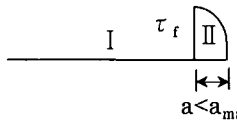

Before interfacial crack ($P<P_{max}$)

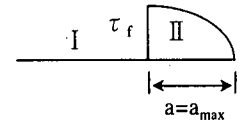

Crack initiation at x=L ($P=P_{max}$)

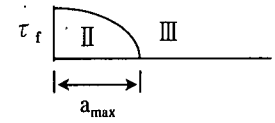

Crack propagation

(c) Model III

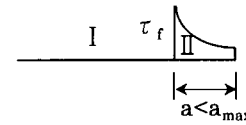

Before interfacial crack

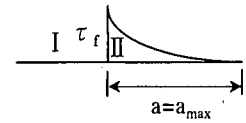

Crack initiation at x=L ($P=0.97P_{max}$)

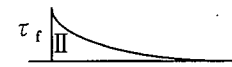

Crack propagation

(d) Model IV

Fig. 4 Different crack propagation mode at simple shear test

(2) Load-carrying capacity

For large values of stress transfer length L, five models assumed give a same formula $P_{max} = \frac{\tau_f b_1}{\lambda}$. It can also be written as

$$P_{max} = b_1 \sqrt{\frac{2G_f}{\frac{1}{E_1 t_1} + \frac{b_1}{b_2 E_2 t_2}}}$$

It can be concluded that load-carrying capacity

of the four $\tau-\delta$ models is the same if the interfacial fracture energy G_f is taken as the same value. It is found that P_{max} is independent of τ_f and δ_f.

(3) Effective stress transfer length

The effective stress transfer (bond) length l_e is defined as the length needed to attain 97% of P_{max} for models Ⅰ, Ⅱ and Ⅳ, and is defined as the length needed to attain P_{max} for models Ⅲ. Taking into account that $\tanh(2)\approx 0.97$, following equations can be derived

$$l_e=\frac{2}{\lambda} \text{ for models Ⅰ and Ⅳ;}$$

$$l_e=a+\frac{1}{2\lambda_1}\ln\frac{\lambda_1+\lambda_2\tan(\lambda_2 a)}{\lambda_1-\lambda_2\tan(\lambda_2 a)} \text{ for model Ⅱ,}$$

where $a=\frac{1}{\lambda_2}\arcsin\left[0.97\sqrt{\frac{\delta_f-\delta_1}{\delta_f}}\right]$;

$$l_e=\frac{\pi}{2\lambda} \text{ for model Ⅲ}$$

Following gives a numerical solution for the case of one layer carbon FRP sheet bonded on a concrete plate. The material properties and sizes of structure model are given as follows:

$t_1=0.111\,\text{mm}$, $t_2=60\,\text{mm}$, $b_1=100\,\text{mm}$, $b_2=300\,\text{mm}$, $L=150\,\text{mm}$, $E_1=2.3\times10^5\,\text{MPa}$, $E_2=3.25\times10^4\,\text{MPa}$, $\delta_f=0.2\,\text{mm}$, $\delta_1=0.02\,\text{mm}$, $\tau_f=4.5\,\text{MPa}$, $G_f=0.45\,\text{N/mm}$.

The numerical calculation results of effective bond length are 67.2 mm, 48.5 mm, 52.8 mm, 67.2 mm, respectively. The computation value of maximum load is 15121kN.

The relation between the maximum transferable load (load-carrying capacity) and interfacial fracture energy, the relation between the maximum transferable load and thickness of FRP, and the relation between the maximum transferable load and Young's modulus of FRP are shown in **Fig. 5-7**, respectively for the case of $l>l_e$. In **Fig. 8**, the maximum transferable load is expressed as a function of total bond length L. Variations of

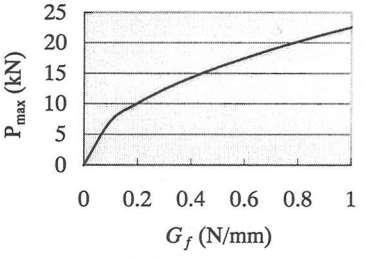

Fig. 5 Relation between P_{max} and G_f

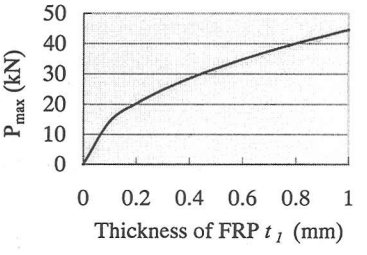

Fig. 6 Relation between P_{max} and t_1

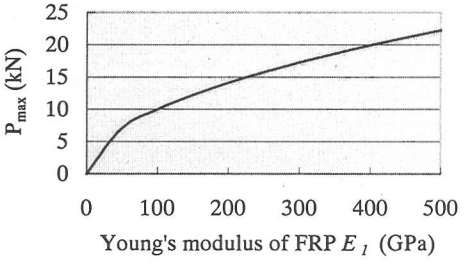

Fig. 7 Relation between P_{max} and E_1

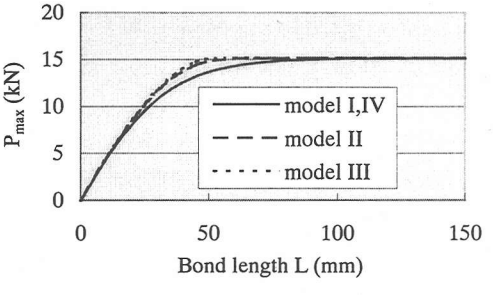

Fig. 8 Relation between P_{max} and bonding length L

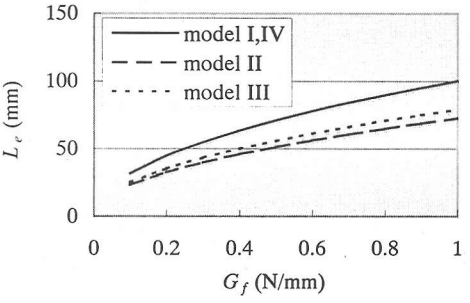

Fig. 9 Relation between L_e and G_f

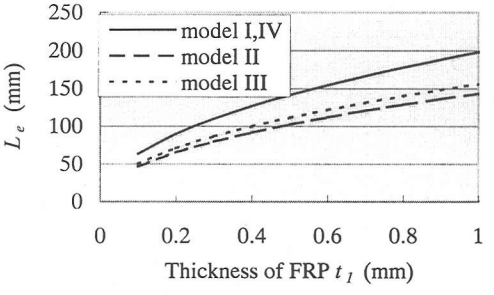

Fig. 10 Relation between L_e and t_1

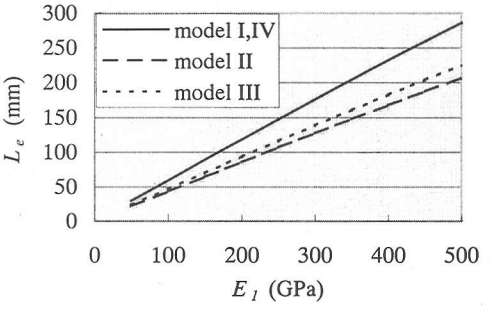

Fig. 11 Relation between L_e and E_1

effective bond length with interfacial fracture energy, thickness of FRP and Young's modulus of FRP are shown as in **Fig. 9-11**, respectively. It is found that P_{max} and l_e increase with the increase of interfacial fracture energy G_f and FRP stiffness (FRP thickness t_1 times FRP Young's modulus E_1).

5. CONCLUSIONS

In this paper, a nonlinear fracture mechanics approach has been introduced to derive theoretical solutions on interfacial stress transfer of the adhesive bonded joint. The nonlinear behavior is modeled by using four kinds of assumed shear stress-slip curves. The numerical simulations indicate that this method can be used to predict fracturing procedure such as initiation of micro-cracking and cracking (debonding), cracking propagation, shear stress distribution and load-carrying capacity along laminate-concrete interface. The following conclusions can be made.

1) The derived expressions for the maximum transferable load (load-carrying capacity) have a same form, which is only dependent on the value of interfacial fracture energy, thickness and Young's modulus of laminates, even different stress-slip models are considered, if the bond length is relatively large (larger than effective bond length).
2) Load-carrying capacity increases with the increase of interfacial fracture energy, thickness of laminate and Young's modulus of laminate.
3) Effective bond length is dependent on the value of λ, which may be varied by the different bond strength (shear stress peak) τ_f, interfacial fracture energy and shear stress-slip curves. Effective bond length increases with the increase of interfacial fracture energy, thickness and Young's modulus of laminate.
4) Shear stress-slip curves significantly affects the debonding propagation, shear stress distribution along the interface, and elastic-softening-debonding region and effective bond length.
5) The derived solutions can be used to predict the debonding behavior and debonding failure of steel/FRP strengthened concrete structures by comparing with the experimental results.

REFERENCES

1) Buyukozturk, O. and Hearing, B.: *Failure behavior of precracked concrete beams retrofitted with FRP*, Journal of Composites for Construction, ASCE, Vol. 2, No. 3, pp.138-144, 1998.
2) Täljsten, B.: *Strengthening of concrete prisms using the plate-bonding technique*, International Journal of Fracture, 82, pp.253-266, 1996.
3) Täljsten, B.: *Strengthening of beams by plate bonding*, Journal of Materials in Civil Engineering, ASCE, Vol. 9, No. 4, pp.206-212, 1997.
4) Roberts, T. M.: *Shear and normal stresses in adhesive joints*, Journal of Engineering Mechanics, ASCE, Vol. 115,

No. 11, pp.2460-2479, 1989.

5) Roberts, T. M.: *Approximate analysis of shear and normal stress concentrations in the adhesive layer of plated RC beam*, The Structural Engineer, Vol. 67, No. 12, pp.229-233, 1989.

6) Brosens, K. and Gemert, D. V.: *Plate end shear design for external CFRP laminates*, Fracture Mechanics of Concrete Structures, Proceedings FRAMCOS-3, pp.1793-1804, 1998, AEDIFICATIO Publishers, D-79104 Freiburg, Germany.

7) Triantafillou, T. C.: *Fracture mechanics approaches to concrete strengthening using FRP materials*, Fracture Mechanics of Concrete Structures, Proceedings FRAMCOS-3, pp. 1761-1770, AEDIFICATIO Publishers, D-79104 Freiburg, Germany.

8) Saadatmanesh, H. and Malek, A. M.: *Prediction of shear and peeling stresses at the plate ends of beams strengthened with FRP plates*, Non-Metallic (FRP) Reinforcement for Concrete Structures, Proceedings of the Third International Symposium, Vol. 1, pp.311-318, Oct., 1997.

9) Malek, A. M., Saadatmanesh, H. and Ehsani, M. R.: *Prediction of failure load of R/C beams strengthened with FRP plate due to stress concentration at the plate end*, ACI Structural Journal, Vol. 95, No. 1, pp.142-152, 1998.

10) Wu, Z. S. and Yoshizawa, H.: *Analytical/Experimental study on composite behavior in strengthening structures with bonded carbon fiber sheets*, Journal of Reinforced Plastics and Composites, Vol. 18, No. 2, pp.1131-1155, 1999.

11) Yin, J. and Wu, Z. S.: *Interface crack propagation in FRP-strengthening structures using nonlinear fracture mechanics*, 4th International Symposium on Fiber Reinforced Polymer for Reinforced Concrete Structures, SP-188, ACI International, pp.1035-1047, Oct. 31-Novem. 5, 1999, Baltimore.

12) Nishida, H., Kamiharako, A., Shimomura, T. and Maruyama, K.: Bond Mechanism between continuous fiber and concrete, Proceedings of the Japan Concrete Institute, Vol. 21, No. 3, pp.1507-1512, 1999 (In Japanese).

13) Kamiharako, A., Shimomura, T., Maruyama, K. and Nishida, H.: *Analysis of bond and debonding behavior of continuous fiber sheet bonded on concrete*, Journal of Materials, Concrete Structures and Pavements, JSCE, Vol. 45, No. 634, pp.197-208, November, 1999 (In Japanese).

14) Sato, Y., Asano, Y. and Ueda, T.: *Fundamental study on bond mechanism of carbon fiber sheet*, Journal of Materials, Concrete Structures and Pavements, JSCE, Vol. 47, No. 648, pp.71-87, May, 2000 (In Japanese).

15) Yoshikawa, H. and Tanabe, T.: *An analytical study of the tension stiffness of reinforced concrete members on the basis of bond-slip mechanism*, Transactions of the Japan Concrete Institute, Vol. 8, pp. 473-480, 1986.

16) Vandewalle, L.: *Cracking behavior of reinforced concrete members*, The second East Asia-Pacific Conference on Structural Engineering & Construction, pp.384-390, 11-13 January, 1989, Chiang Mai.

17) Wu, Z. S.: Development of computation models for reinforced concrete plate and shell element, Doctoral Dissertation, Nagoya University, Nagoya, December, 1989.

18) Wu, Z. S., Yoshikawa, H. and Tanabe, T.: *Tension stiffness model for cracked reinforced concrete*, Journal of Structural Engineering, ASCE, Vol. 117, No. 3, pp.715-732, March, 1991.

(Received December 3, 1999)

外面接着された鋼板/連続繊維シートとコンクリートの界面せん断伝達に関する解析的検討

袁　鴻・呉　智深・吉沢　弘之

連続繊維シート等の補強材とコンクリートの接着界面の応力伝達特性は，それらにより補強された構造物全体の構造性能に大きな影響を与える．特に，接着界面の剥離進展により，補強された構造物の耐荷力や変形性能を大きく低下させることがあるため，接着界面のせん断変形挙動および剥離現象の解明は重要な問題となっている．本研究では，幾かの簡易な線形・非線型式を想定した場合の接着界面の局所せん断応力 τ と相対変位 δ の関係に対して，接着界面のせん断応力分布および補強材のひずみ分布に関する理論式を剥離破壊エネルギーの概念を用いて系統的に導いた．また，最大剥離荷重，せん断応力の有効伝達長さ，剥離の生成・進展に関する検討を行い，界面せん断伝達メカニズムを解明した．